Depth and Transient Imaging with Compressive SPAD Array Cameras Supplementary Material

Qilin Sun Xiong Dun Yifan Peng Wolfgang Heidrich
King Abdullah University of Science and Technology

In this supplement we present additional details and results for the methods presented in the main text. Specifically, we present

- An additional result of transient imaging (Section 1)
- Experiments regarding the impact of the temporal PSF model on reconstruction quality (Section 2)
- Details on the capture workflow (Section 3)
- A full description on of the optical setup (Section 4), including the microlens array (Section 5).

1. Additional Results

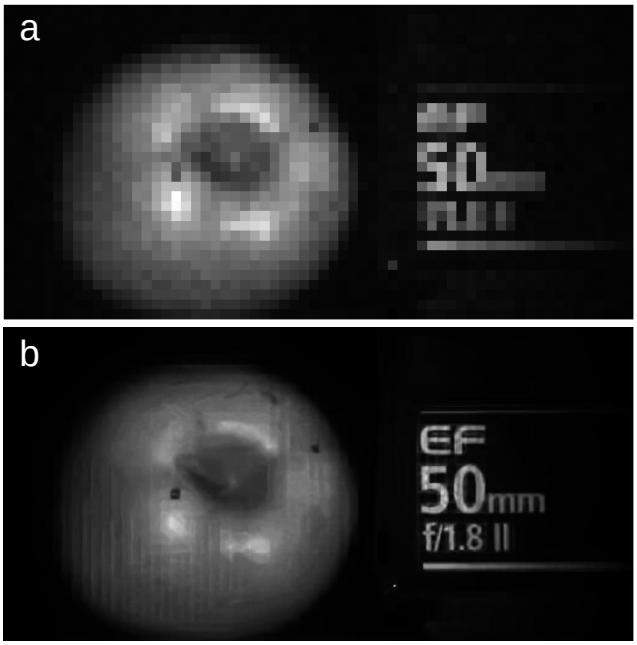

Figure 1. **Additional Result of Spatial Resolution Improvement** (a) Raw data modulated by the first random pattern. (b) Reconstructed Intensity Map.

Figure 1 shows the result of a reconstructed intensity map. As we can observe that the details of the characters and apple are finely reconstructed.

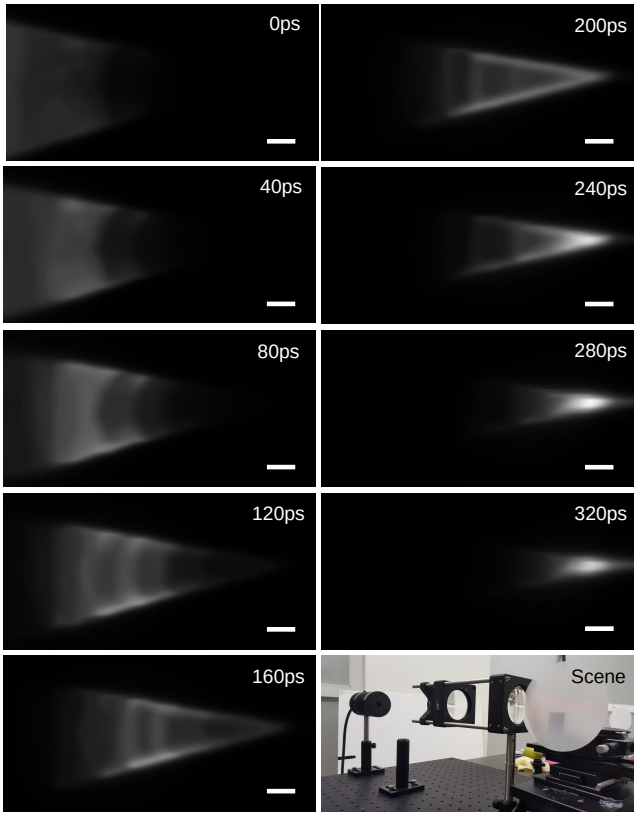

Figure 2. **Light Concentrated by a Lens**
We here present one frame of every two frames.

Figure 2 shows a re-creation of an iconic scene for light-in-flight imaging by Abramson [1]. A convex lens (50.8mm diameter, 75mm focal length) focuses a short pulse of light into a point. To visualize this light propagation, a diffusing screen was lines up with the optical axis of the lens, showing a 2D cross-section of the 3D light cone (see lower right of Figure 2. While the resolution achieved with our system does not match that of Abramson's holographic approach, it is significantly than what could be achieved with regular time of flight cameras.

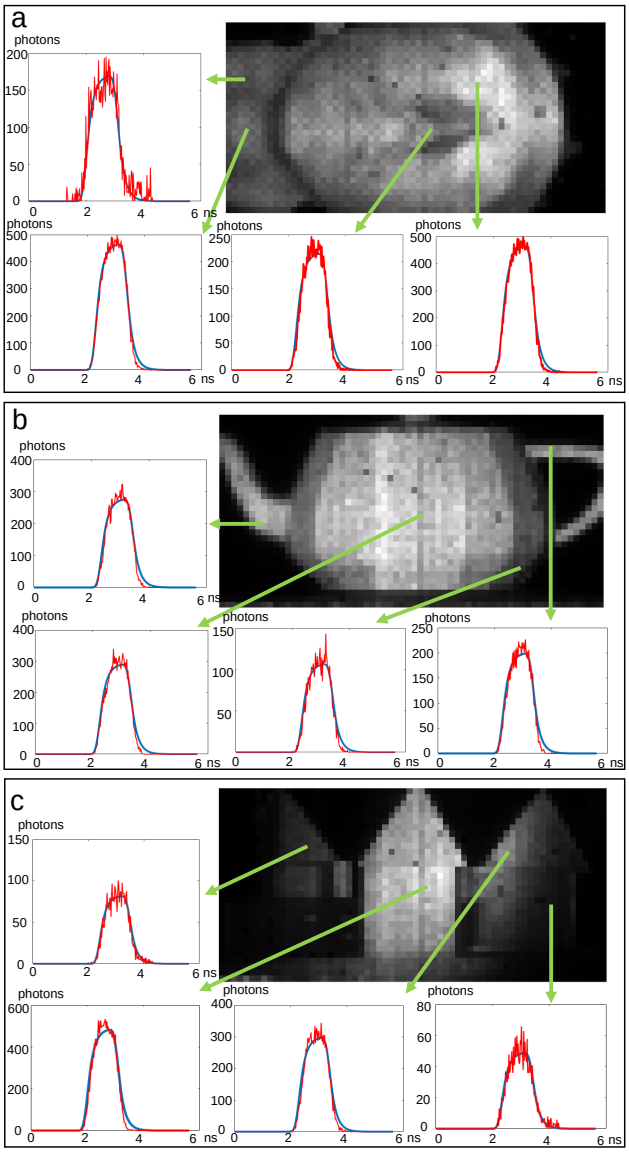

Figure 3. **Analyzing the quality of the temporal PSF model.** For different image pixel, we show the time profiles of the captured raw data (red) as well as the fitted temporal PSF (blue). The time profiles correspond to a single random pattern from the compressive sensing approach.

2. Temporal PSF Model

Details of Temporal PSF Model As mentioned in the main text, the time histograms captured using TCSPC technique are the convolution of gate signal and received laser pulse with our considering noise and signal distortion. Our target is to extract the phase and amplitude information of the laser pulses. Hence, we propose a model-based temporal deconvolution method to reconstruct the laser pulses' time histograms. To fit the time histogram better, we take the physical electronic response into consideration such as RC response of high frequency signal, low pass filter effect of electronics and time jitter. We can obtain our gate signals model by the following procedure. Firstly, we can obtain the RC response of a ideal gate signal

$$\mathbf{\Pi}_{RC}(t) = \begin{cases} 1 - e^{-t/RC} & 0 < t \leq t_0 \\ (1 - e^{-t_0/RC})e^{-t/RC} & t > t_0 \end{cases} \quad (1)$$

Where t_0 means 1ns. Then we use Gaussian a low pass filter to remove the high frequency component of $\mathbf{\Pi}_{RC}(t)$ and get our gate model $\mathbf{\Pi}$. We guessed a group of RC parameters to fit the data well. Finally, We fit the data well when R and C are 3.5Ω and 5pF respectively. Fortunately, those two parameters are globally suitable to all the data as illustrated in Figure 3.

Model Testing As is illustrated in Figure 3 the background noise and dark counts shown in the three scene figures(summed over time axis) have been removed. The three groups of data are all modulated by the first random pattern in convenient of comparison. Although the overall fit is quite good, there is a slight discrepancy in the tail region of the PSF. We speculate that this could be due to a slightly non-Gaussian shape of the picosecond laser pulse. Fortunately, this slight mismatch does not seem to have a major influence the reconstruction quality.

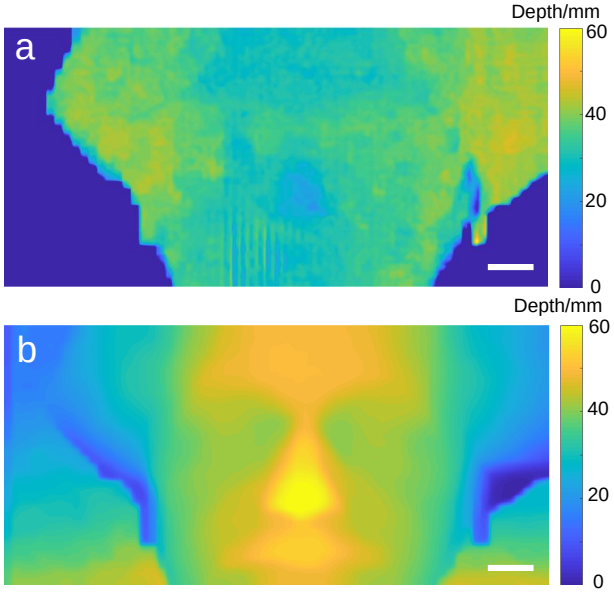

Figure 4. **Comparison of depth imaging results with and without temporal deconvolution.**

Comparison Figure 4 shows the results of a depth reconstruction with and without temporal deconvolution. By comparing Figure 4a and Figure 4b, we can find that most

of the depth details cannot be resolved without temporal deconvolution while the fine depth details are well resolved.

Transient Imaging without Temporal Deconvolution Next, we test the impact of the temporal deconvolution on the quality of the transient imaging results. In Figure 5, we show light-in-flight imaging result from Figure 7 of the main text without our temporal deconvolution. We can observe that light pulses are reconstructed as very long streaks, and the phase relationship between different frames is not very obvious. Compared with the result with temporal deconvolution in the paper, our fitting method drastically improved the phase accuracy and gives a right pulse duration based on the physical parameters of the picosecond laser.

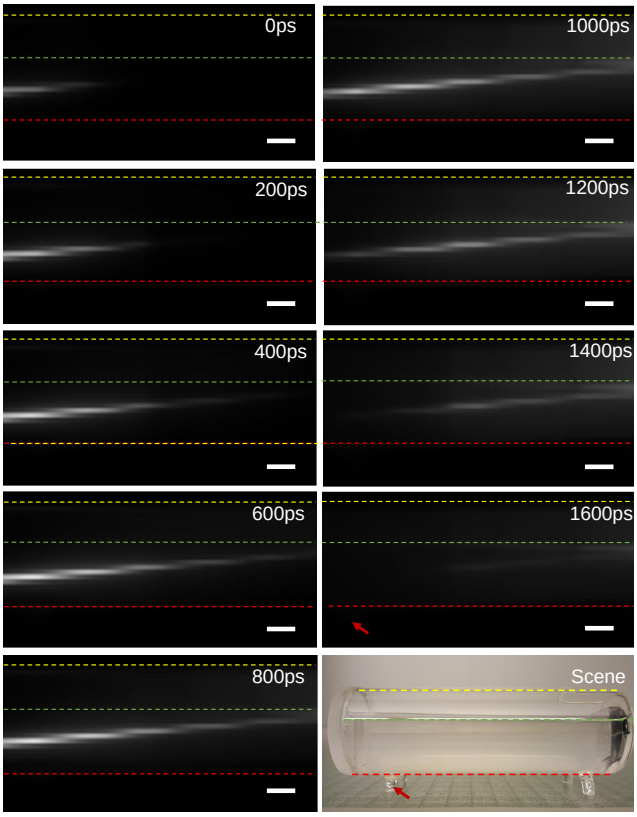

Figure 5. **Light-in-flight imaging result without temporal deconvolution.**

3. System Work Flow

The system works as the following working flow and is illustrated in Figure 6. First, a random pattern frame generated by Matlab is sent to DLP4500 control board through HDMI interface. Following a trigger signal is sent through USB port to DLP4500 control board to enable a random pattern to be displayed on the DMD. Then the SPAD sensor array is activated to capture a series of data frames

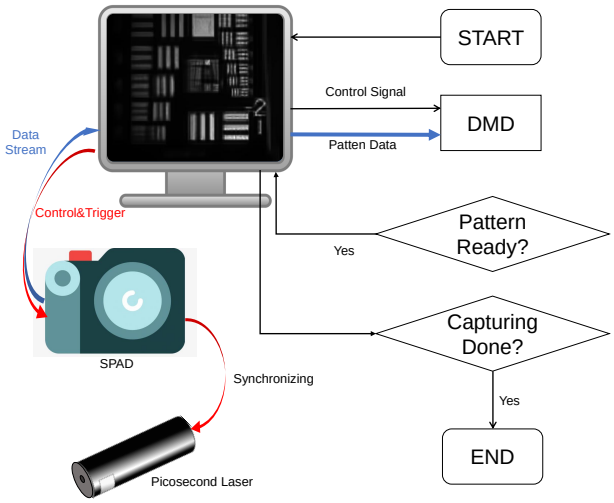

Figure 6. **System work flow**

that are modulated by the random pattern displayed on the DMD. Meanwhile, the scene is illuminated by picosecond laser which is triggered by 50MHz synchronizing signal generated by the built-in Xilinx FPGA of the SPAD camera. Since the 50MHz synchronizing signal generated by FPGA is TTL while the required triggering signal is NIM, we finally use SIA 400 module to invert and attenuate TTL pulses to NIM pulses. After integrating sufficient frames at a certain phase, the SPAD camera shifts the gate window(20ps delay referring to the rising edge of the clock signal) and captures another integrated frames until covering all phases.

After all of the data being captured, they are transferred back to the controlling system. Then, it starts the next capturing loop modulated by a new random pattern until covering all the 100 designed patterns. At last, we capture 20 groups of data under a pattern with all micromirror switched off to calibrate the background light and hot pixels. The whole capturing process lasts around 9 minutes.

4. Details of the Optical Setup

As shown in Figure 7a and b, the imaging system consists of an 85mm Cannon imaging lens, DMD optical system 8, inverted 0.9X Edmund Platinum double side telecentric lens, diffractive microlens array and MPD-SPC3 SPAD array. We insert a Semrock 655/15nm bandpass filter behind the imaging lens to remove most ambient light.

The principal ray incidents into the TIR-prism and is refracted at the two surfaces as shown in Figure 8. Later, all the light has an approximate 24° with the micromirrors at the "On" state and is reflected out by the right angle prism part. We utilize an inverted 0.9X double side telecentric lens as the re-imaging lens such that 1 pixel of the SPAD array(pixel size 150μm) is corresponding to 12.5 micromir-

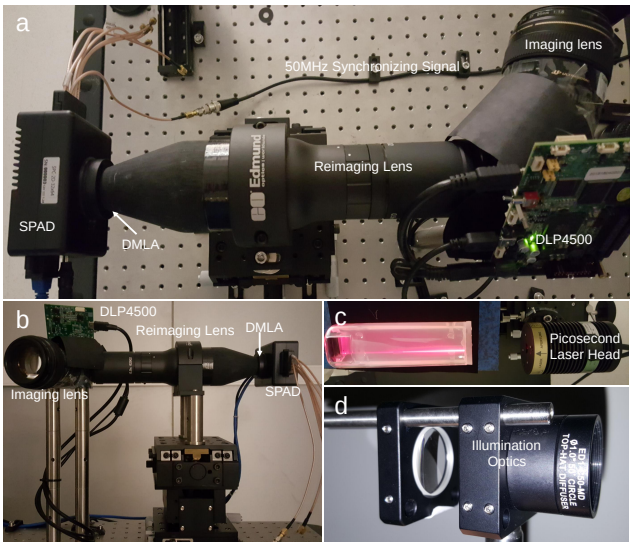

Figure 7. Prototype of Imaging System: (a) Top view of our imaging system. (b) Side view of our imaging system. (c) Scene of light propagating in the milked water. (d) Illuminating optics with a diffuser and a 30mm biconvex lens.

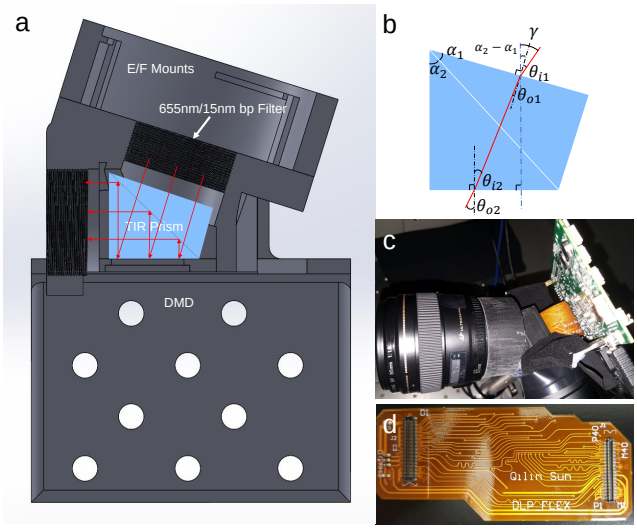

Figure 8. DMD Optical System: (a) Sectional view of our DLP optical system. (b) Details about how to determine the imaging lens axis angle. (c)3D printed prototype of the DLP optical system. (d) Our designed DMD flex cable for the Prototype.

rors on DMD(pixel size 10.8μm). Finally, the light is concentrated by the diffractive microlens array on to the active area of the SPAD sensor.

For easy adjustment of rotation and focus, we fix the re-imaging lens and SPAD camera on an XYZ stage and a Goniometers(Optics-Focus MAG-130-10) as shown in Figure 7b. The connecting part between the re-imaging lens and SPAD camera is our 3D printed M62$\times$0.75 to C-mount converter. Figure 7c shows the top view of the capturing scene of "light-in-flight" imaging. The laser pulses are repetitively sent and propagate in the glass pile filled with slightly milked water. Figure 7d shows the illuminating optics. To illuminate the 3D scene smoothly, we use a diffuser to diffuse the laser pulses. Considering the weak power of our laser, we put a 30mm biconvex lens to concentrate the laser pulses into a certain area in case of reducing the illumination light power too much. By the way, considering the costs of the system, we use a relatively low cost picosecond laser head (around 3000 euros) with center wavelength 655nm and pulse energy only 40pJ instead of a high pulse energy blue laser where the SPAD array has a much higher photon detection efficiency.

Figure 8 illustrates the details of the DMD optical system. We designed E/F Mounts to install the imaging lens with $\gamma = 17.43°$ between the optical axis of the imaging lens and the normal direction of DMD surface. As is shown in Figure 8b, the apex angle α_1 and α_2 are 33° and 45° respectively. As the incident light for the DMD required is $\theta_{o2} = 24°$, we could obtain the angle γ through following equations.

$$\begin{cases} sin\theta_{i1} = n_{BK7} sin\theta_{o1} \\ \theta_{i2} = \theta_{o1} + \alpha_2 - \alpha_1 \\ n_{BK7} sin\theta_{i2} = sin\theta_{o2} \\ \gamma = \alpha_2 - \alpha_1 + \theta_{i1} \end{cases} \tag{2}$$

Where the refractive index n_{BK7} of the BK7 glass of the TIR prism at 655nm is 1.5144.

Figure 8c shows our assembled prototype. The mechanical part is fabricated by Objet260 3D printer using $veroBlack^+$ material. In addition, to make the electronics of the DMD system more stable and easy to assemble, we designed and fabricated a 4 layer FPC flex cable for DMD.

5. Diffractive Microlens Array

The low fill factor of our SPAD array will make the compressive sensing scenario ill-conditioned because the detector itself cannot obtain all the needed information modulated by the corresponding patch on the DMD. To deal with this condition, we tried to design different kinds of microlens arrays including achromatic microlens array, 2π period DMLA [2] and 4π period DMLA. We fabricated achromatic microlens array and 4π period DMLA using NanoScribe with IP-S photoresist. Differently, we fabricated 2π period DMLA(2^4 phase level structure) using 0.7μm direct laser writing with SU-8 photoresist and etched the pattern onto the silica wafer by RIE etching. After installing the glass for the bare SPAD sensor, we measured the distance between the glass window surface and the sensor surface. According to the measured data, we designed the microlens

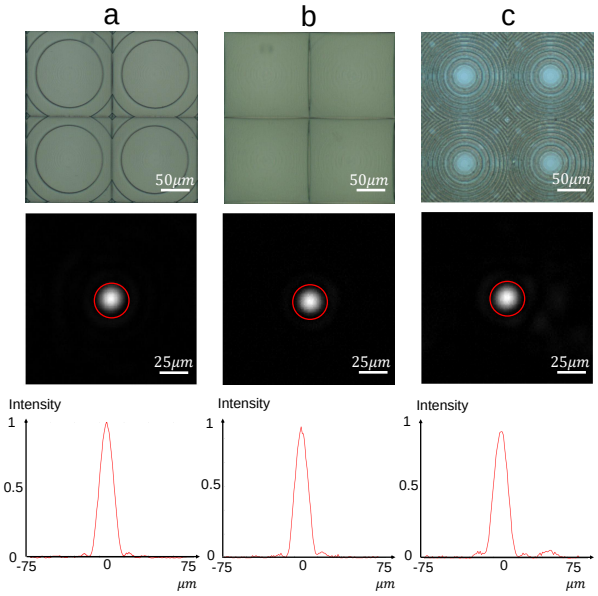

Figure 9. **Comparison of our MLAs** We show the fabricated results taken by microscopy, focal spots of the microlens recorded on a CMOS camera and the intensity distribution along the center latitude respectively. (a) Diffractive microlens array with 4π period which is fabricated by Nanoscribe using IP-S photoresist. (b)Refractive microlens array which is fabricated by Nanoscribe using IP-S photoresist. We take it as a reference. (c)Diffractive microlens array with 2^4 phase levels structure which is fabricated by 0.7μm direct laser writing.

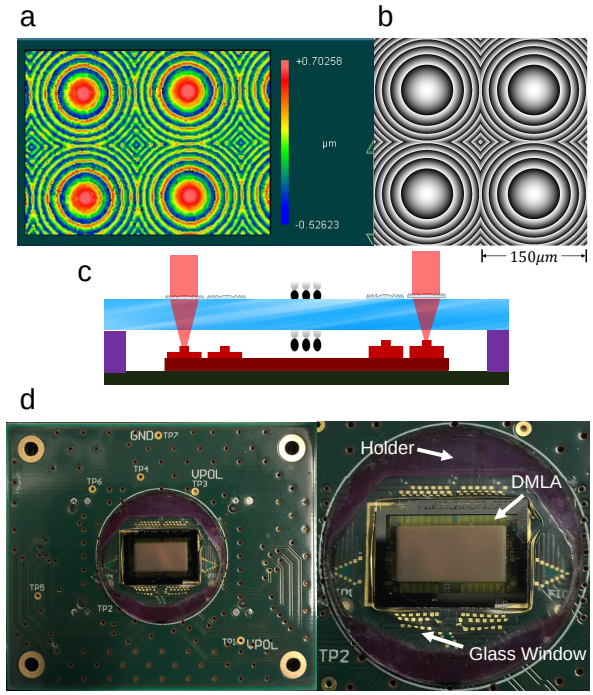

Figure 10. **Illustration of the installation of DMLA** (a) Profile of the fabricated microlens array scanned by Zygo 3D; (b) Profile of the designed microlens array; (c) Illustration of light focusing contribution of the microlens array. Notice that to protect the sensor, we attach a Fused Silica glass with a $0.5mm$ thickness in front of the bare sensor before installing the DMLA. The glass window is supported by a polycarbonate ring and fixed with UV glue. (d) The SPAD sensor installed with our fabricated DMLA.

arrays with focal length 1.035mm. In practice, we can obtain a higher fill factor with a shorter focal length of the microlens. With the powerful fabrication ability of Nanoscribe, we are able to fabricate a microlens with very short focal length. Unfortunately, a micro lens array with short focal length has to be directly installed on the bare sensor, and installing it on a bare sensor is a big challenge to us. Later, we will try to build a lens group array instead of a DMLA or MLA if we can obtain spare sensors.

Figure 9 illustrates different micro lens arrays to improve the fill factor of our SPAD array. Figure 9a shows the 4π period DMLA. It is fabricated by a Nanoscribe and sliced with 50nm distance. The energy marked by red circle is 64.22% of the energy over all the area covered by DMLA patch. In another word, the fill factor is improved 20.44 times. The refractive MLA is designed and optimized for a 150μm patch and its efficiency can reach 64.51% which can be taken as a reference. The the lens surface of the 4π DMLA is s approximated by a modulo zone plate 4π representation from this refractive MLA. Different from the 3D fabricating processing, 2π DMLA consists of 16 phase levels, and hence four successive binary masks($16 = 2^4$) are required to be generated. The alignment between this 4 layer could be a challenge and might contains some error and mixing as shown in Figure 9c. Hence, the efficiency of this MLA is only 52.87%. In addition, the most significant shortcoming of this method compared with the above two is that the low diffractive efficiency might cause interference between neighboring pixels. But the advantage of this method is that we can etch the SU-8 photoresist onto the silica wafer and make the patter more stable and not easy to be scratched.

Considering the stability of the microlens array and avoiding the pattern been scratched by the vacuum head during installing process, we chose to use the 2π period DMLA which has been etched onto the wafer finally.

Figure 10 illustrates the installation of DMLA. We firstly used a polycarbonate ring to support a 0.5mm thick silica glass window. After the protecting glass window was successfully installed and fixed, we used FINEPLACER femto to align the DMLA and the SPAD sensors. Our DMLA and research&development SPAD array offered by MPD were all designed with align marks at the top right and the bottom left corner. Finally, the DMLA was fixed on the glass window using UV optical glue.

References

[1] N. Abramson. Light-in-flight recording: high-speed holographic motion pictures of ultrafast phenomena. *Applied optics*, 22(2):215–232, 1983. 1

[2] G. Intermite, A. McCarthy, R. E. Warburton, X. Ren, F. Villa, R. Lussana, A. J. Waddie, M. R. Taghizadeh, A. Tosi, F. Zappa, et al. Fill-factor improvement of si cmos single-photon avalanche diode detector arrays by integration of diffractive microlens arrays. *Optics express*, 23(26):33777–33791, 2015. 4